American Mineralogist, Volume 82, pages 557–570, 1997

Dislocation formation and albitization in alkali feldspars from the Shap granite

MARTIN R. LEE AND IAN PARSONS

Department of Geology and Geophysics, University of Edinburgh, West Mains Road, Edinburgh EH9 3JW, U.K.

ABSTRACT

Orthoclase-rich alkali feldspars in the Lower Devonian Shap granite, northwest England, contain two generations of albite-rich feldspar. These have partially replaced earlier exsolution microtextures consisting of albite lamellae (coarse semicoherent albite films and fine coherent albite platelets) in tweed orthoclase. The earlier generation of replacive albite-rich feldspar ($\sim Ab_{90}An_9Or_1$) occurs together with orthoclase-rich feldspar ($\sim Ab_{10}Or_{90}$) in veins that crosscut exsolution microtextures throughout grain interiors. This episode of recrystallization was mediated by magmatic fluids at ~410 °C (estimated from two-feldspar geothermometry) and was driven by stored elastic strain energy, which was relatively homogeneously distributed throughout the microtextures. The later generation of replacive albite-rich feldspar, which is restricted to grain margins and is compositionally pure ($Ab_{>99}$), was produced by magmatic-hydrothermal fluids at ~370 °C. This generation of albite-rich feldspar does not crosscut exsolution microtextures and has selectively replaced volumes of highly elastically strained feldspar surrounding edge dislocations along semicoherent albite films. Marked differences in controls of the localization of the two generations of replacive albite-rich feldspar by pre-existing exsolution microtextures indicate that significant numbers of edge dislocations developed along albite films after the first phase of fluid-feldspar interaction and associated albitization but before the second phase. This relation indicates that edge dislocations formed between 410 and 370 °C. These observations have important implications for understanding the factors that control the interaction of alkali feldspars with fluids both in cooling igneous rocks and in clastic sedimentary rocks during diagenesis.

INTRODUCTION

Recent studies of alkali feldspars from slowly cooled igneous rocks have demonstrated that feldspar microtextures are an invaluable source of information on thermal history (Brown et al. 1983; Waldron and Parsons 1992) and the evolution of fluids (Parsons 1978, 1980; Worden et al. 1990; Waldron et al. 1993; Brown and Parsons 1994; Walker et al. 1995). Alkali feldspars readily interact with magmatic fluids at temperatures of <450 °C during cooling. This secondary or deuteric alteration results in the replacement of pristine coherent or semicoherent exsolution microtextures by micropore-rich intergrowths of albite- and orthoclase-rich feldspar subgrains (termed ''patch perthites'' by Parsons 1978). These isochemical replacement reactions are driven by the relaxation of elastic strain energy accumulated as microtextures coarsen and transform during cooling (Brown and Parsons 1993); all alkali feldspars in slowly cooled rocks initially contain this stored elastic strain energy, and so all are potentially reactive. Deuteric alteration is geochemically important because radiogenic-argon leakage (Parsons et al. 1988) and O-isotope exchange (Waldron et al. 1993) may accompany recrystallization. Loss of coherency and formation of interconnected micropore networks also render volumes of deuterically altered feldspar susceptible to weathering, following uplift and exposure, and to diagenetic reactions after erosion and sedimentation (Walker 1990, 1991; Lee and Parsons 1995; Walker et al. 1995). Hydrothermal alteration differs from deuteric alteration by occurring in chemically distinct fluids originating outside the host rock, for example from the envelope of an igneous intrusion. As a consequence, substantial bulk chemical changes may accompany microtextural coarsening during hydrothermal alteration.

Most microtextural investigations of deuteric alteration have focused on feldspars that were initially largely coherent crypto- and microperthites of median bulk composition from hypersolvus syenites (Parsons 1978, 1980; Worden et al. 1990; Waldron and Parsons 1992). Although compositional and microtextural changes arising from deuteric alteration of these feldspars are now well understood, several questions remain. In particular, in many instances, grain boundaries and intragranular microtextures appear to exert little control on interaction with deuteric fluids (Worden et al. 1990). However, where coherent cryptoperthites have coarsened and partially lost coherency (for example by the formation of pleated rims at intergranular boundaries; Lee et al. 1997), alkali feld-

0003–004X/97/0506–0557$05.00

TABLE 1. Summary of the characteristics of the four microtexturally distinct varieties of albite-rich feldspar in Shap granite phenocrysts

Variety of albite-rich feldspar	Occurrence	Microtexture	Bulk molecular composition
Coherent albite platelets	In narrow bands of cryptoperthite within microperthites	<75 nm wide exsolution lamellae	Assumed $\sim Ab_{100}$
Semicoherent albite films	In microperthites throughout grain interiors	>75 nm wide by many micrometers long exsolution lamellae	Assumed $\sim Ab_{100}$
Veins of patch perthite albite	Throughout grain interiors	Anastomosing veins cutting microperthites	$Or_{1.5}Ab_{89.8}An_{8.7}$
Pure replacive albite	Only within ~1 mm of intergranular boundaries	Volumes selectively replacing semicoherent albite films	$Or_{0.7}Ab_{99.1}An_{0.2}$

spars react more readily with fluids. This implies that the character of microtextures close to grain boundaries, in particular their coherency, may control interaction of fluids with feldspars.

This paper describes results of a study of alteration microtextures in orthoclase-rich alkali feldspars from the Lower Devonian Shap granite, northwest England. Our aim was to determine the mechanisms by which pristine exsolution microtextures, and in particular the stored elastic strain energy associated with them, control interaction of relatively low temperature deuteric-hydrothermal fluids with alkali feldspars. Previous work has shown that pristine exsolution microtextures in these feldspars comprise cryptoperthites (made of small coherent albite lamellae, called platelets, in tweed orthoclase) and microperthites (made of coarser semicoherent albite lamellae, called films, in tweed orthoclase) (Lee et al. 1995). These exsolution microtextures were partially replaced by two compositionally and microtexturally distinct generations of albite-rich feldspar. The earlier generation (bulk composition $\sim Ab_{90}$) exists together with orthoclase-rich feldspar in anastomosing veins throughout grain interiors (Lee et al. 1995; Lee and Parsons 1995). In this paper we concentrate on a second and later generation of replacive albite-rich feldspar that is distinguished by its compositional purity ($Ab_{>99}$) and close association with semicoherent albite films. The near end-member chemical composition of this albite-rich feldspar is typical of diagenetic albite in sedimentary rocks (Kastner 1971; Kastner and Siever 1979) and may therefore indicate that fluid-feldspar interaction took place at low temperature, late in or subsequent to the cooling history of the pluton. Shap granite alkali feldspars have therefore experienced two separate phases of fluid-feldspar interaction, which have produced compositionally and microtexturally distinct reaction products. The implications are that the manner in which alkali feldspars interact with fluids may depend on the temperature and origin of ambient fluids. Characteristics of all four varieties of albite-rich feldspar which occur in Shap alkali feldspars are summarized in Table 1.

EXPERIMENTAL METHODS

Shap granite alkali feldspars were studied using a range of complementary imaging and analytical techniques. They were initially characterized in thin section by light microscopy and then by backscattered electron (BSE) imaging using a Cambridge Instruments S250 scanning electron microscope (SEM) operated at 20kV. Chemical analyses were obtained using a Cameca Camebax WDS electron probe operated at 20kV with a 10nA beam current. To obtain bulk analyses of microtextures and also to minimize Na loss, the electron beam was rastered over an area of $\sim 20\ \mu m^2$. The luminescence color of microtextures was noted during electron probe analysis.

Areas of interest identified by light and BSE microscopy and electron probe analysis were then prepared for transmission electron microscopy (TEM). Copper discs with a central hole 600-800 μm in diameter were attached to the surface of the thin section with an epoxy resin, the central hole being positioned over the area of interest. After the resin had cured, the disc with feldspar attached was removed from the thin section and ion-beam thinned until electron transparent. The thinned foils were mounted in a double tilt goniometer specimen holder and studied using a Philips CM12 TEM operated at 120kV. The TEM is equipped with a Gatan image intensifier to aid high-resolution imaging.

Feldspars were also examined using a hydrofluoric (HF) acid vapor-etching technique described by Waldron et al. (1994). Mechanically produced cleavage fragments of phenocrysts were mounted on Al specimen stubs, ultrasonically cleaned, and then suspended ~20 mm above a small volume of HF acid for ~50 seconds. The etched cleavage surfaces were then ultrasonically cleaned and imaged using secondary electrons (SE) in the SEM. On (001) cleavage surfaces HF acid vapor etches orthoclase more rapidly than albite, which stands in relief. This technique is also sensitive to the presence of dislocations because the highly elastically strained feldspar surrounding them dissolves rapidly to form submicrometer-sized etch pits.

Mineralogy of the Shap granite

The Shap granite is a Lower Devonian, subsolvus, biotite-granite intrusion that crops out to the south of Shap, on the eastern margin of the English Lake District. The petrology of the granite has been described by Harker and Marr (1891), Grantham (1928), and Caunt (1986). Grantham (1928) divided the granite into several stages. The samples studied here are from the dominant Stage II gran-

TABLE 2. Bulk molecular compositions of feldspar microtextures and minerals from the Shap granite (determined by electron probe analysis)

	Mole percent			
	Or	Ab	An	*n*
		Pristine microtextures		
Phenocryst				
Interior cryptoperthite	68.0(2.1)	31.1(2.0)	0.8(0.3)	13
Microperthite	71.8(2.6)	27.6(2.5)	0.6(0.2)	15
Cryptoperthite rim	85.9(1.1)	13.9(1.1)	0.2(0.1)	10
Pristine feldspar between thickened albite films	84.8(1.1)	14.9(1.1)	0.3(0.1)	5
Groundmass crystal				
Cryptoperthite rim	85.5(1.2)	14.4(1.1)	0.2(0.1)	8
		Alteration microtextures		
Phenocryst				
Orthoclase-rich patch perthite	90.4(3.8)	9.4(3.8)	0.3(0.2)	22
Albite-rich patch perthite	1.5(0.6)	89.8(5.2)	8.7(5.1)	34
Pure replacive albite	0.7(0.4)	99.1(0.4)	0.2(0.1)	46
Thickened microperthite	72.4(2.6)	27.1(2.5)	0.5(0.1)	20
Groundmass crystal				
Pure replacive albite	0.5(0.2)	99.2(0.4)	0.3(0.2)	20
		Free oligoclase		
Inclusions in phenocrysts	1.7(0.4)	71.8(1.2)	26.5(1.3)	7
Groundmass crystals	2.3(0.4)	72.9(3.1)	24.8(2.8)	8

Note: Figures in parentheses are standard deviations of groups of analyses. *n* denotes number of analyses.

ite, an adamellite containing distinctive coarse pink alkali feldspar phenocrysts, ≤50 mm in size, that comprise ~23 vol% of the rock. These phenocrysts lie in a groundmass of smaller (≤2 mm) pink alkali feldspars, partially chloritized biotite, partially sericitized free oligoclase (~Ab_{73}, Table 2), and quartz. Poikilitically enclosed by the phenocrysts are submillimeter-sized inclusions of partially chloritized biotite, partially sericitized nonperthitic oligoclase (~Ab_{72}, Table 2), quartz, and titanite. Groundmass alkali feldspars are free of such inclusions. The microtexture of Shap granite alkali feldspar phenocrysts has been described by Lee et al. (1995), Lee and Parsons (1995; 1997), and Cox et al. (1996), and is summarized below.

Alkali feldspar microtextures

Previous work has identified three distinct microtextures in phenocrysts and groundmass crystals: (1) pristine cryptoperthite with fine albite platelets, (2) pristine microperthite with coarser albite films, and (3) micropore-rich veins of patch perthite comprising subgrains of albite- and orthoclase-rich feldspar (Lee et al. 1995; Lee and Parsons 1995; 1997). Pristine crypto- and microperthites are made of exsolution lamellae of albite oriented close to ($\bar{6}01$) in tweed orthoclase. The tweed orthoclase consists of very small, ordered-antiordered, twinlike domains that are energetically stranded; the decrease in free energy resulting from further Si-Al ordering is balanced by an increase in strain energy of the domain microtexture (Eggleton and Buseck 1980). The elastic strain energy stored in tweed orthoclase can reach 2–3 kJ/mol (Brown and Parsons 1993). Cryptoperthites and microperthites differ in the abundance, coherency, and size of their exsolution lamellae. Within phenocrysts, these microtextural differences correspond with contrasts in mean bulk molecular compositions (Table 2).

Cryptoperthites occur in three contexts: (1) throughout the interior of phenocrysts as narrow (~30–60 μm wide) zones within microperthites (average bulk composition ~Or_{68}) (Lee and Parsons 1997), (2) as narrow (~10 μm) and discontinuous rims on phenocrysts (~Or_{86}), and (3) as wider (~40–50 μm) rims on groundmass crystals (~Or_{86}) (Table 2). All cryptoperthites contain small (<75 nm wide by a few micrometers long) albite lamellae (platelets) that have fully coherent interfaces with surrounding tweed orthoclase (i.e., the Al-Si-O framework is continuous across the exsolution interface) (Lee et al. 1995). Owing to the difference in unit-cell parameters of unstrained albite and orthoclase at room temperature (e.g., the spacing of 020 lattice planes in low albite is 98.5% of the spacing of equivalent lattice planes in orthoclase), the lattice of albite must be under considerable elastic strain to maintain coherency (i.e., the 020 lattice interplanar spacing of albite has to be stretched by ~1.5%). Brown and Parsons (1993) calculated the stored elastic strain energy of coherent cryptoperthites to be ~2.5–4.0 kJ/mol, depending on bulk composition.

Pristine microperthite is the dominant microtexture in phenocrysts, although it has been extensively altered in groundmass crystals. Microperthites contain coarse albite lamellae (films) that are >75 to ~500 nm in width by many micrometers in length and albite- or pericline-twinned or both. Adjacent films are spaced ~1.0–1.5 μm apart. The size of these films means that, at room temperature, the lattice of albite cannot be strained sufficiently to maintain coherency along the entire length of the exsolution interface. Strain energy at the interface is partially reduced by semiperiodically spaced pairs of edge

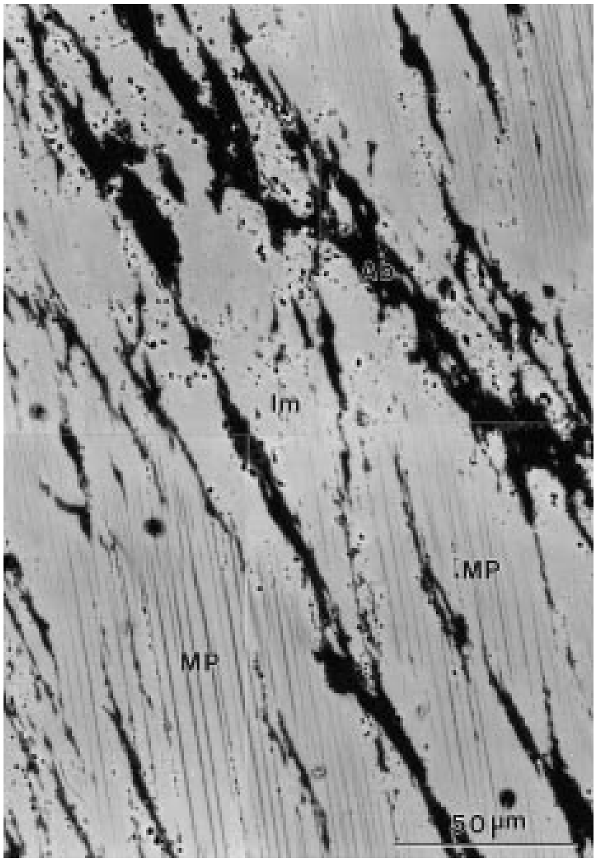

FIGURE 1. Collage of BSE images (obtained by SEM) of the interior of an alkali feldspar phenocryst. Pristine lamellar microperthites (MP) are crosscut by micropore-rich patch perthite veins oriented NW-SE across the micrograph. These veins comprise an intergrowth of albite (black, Ab) and irregular microcline (light grey, Im) subgrains. The irregular microcline subgrains are difficult to distinguish from tweed orthoclase as both phases are similar in mean atomic number.

dislocations that straddle the films (albite films are thus semicoherent). Because of the strain energy introduced in the crystal structure surrounding the missing lattice plane, distinctive pairs of etch pits form at edge-dislocation outcrops during HF acid etching (Waldron et al. 1994). Each pair of edge dislocations represents a section through a continuous dislocation loop that encircles the films (see Lee et al. 1995, Fig. 16). Dislocation loops are present in two orientations, one normal to (010), the other normal to (001), and so in three dimensions the surfaces of semicoherent albite films are covered by an orthogonal network of dislocations on the Murchison plane $\sim(\bar{6}01)$. The spacing of edge-dislocation pairs along the exsolution interface ($\sim$500 nm) is only sufficient, however, to reduce the 1.5% difference in 020 lattice spacings of albite and orthoclase by $\sim$0.1%; the remaining $\sim$1.4% is accommodated by nearly homogeneous elastic strain in the albite structure between dislocations.

Patch perthites comprise anastomosing micropore-rich veins of semicoherent or incoherent subgrains of albite-rich feldspar (low albite) and orthoclase-rich feldspar (irregular microcline) (Fig. 1; Lee et al. 1995). Obtaining bulk chemical compositions of entire patch perthite veins was difficult because of their size and heterogeneity, but electron probe analyses of individual albite- and orthoclase-rich volumes within veins shows that neither component is compositionally pure (Table 2). The albite-rich component of the veins luminesces bright blue under the electron beam. These veins occur throughout phenocrysts, where they predominantly crosscut exsolution microtextures (Fig. 1), but are less common in groundmass crystals. In some cases, patch perthite veins extend from the interior of phenocrysts to inter- and intragranular boundaries. The crosscutting nature of these patch perthite veins and the composition of their constituent albite subgrains (see below) indicate that they have formed by fluid-mediated replacement of pristine microtextures.

Of the three microtexturally distinct varieties of albite-rich feldspar that have been described previously from

→

FIGURE 2. Images of pure replacive albite from the Shap granite. (**a**) Light micrograph (crossed polarizers) of an alkali feldspar grain in the groundmass of the granite. Several patches of pure replacive albite (PRA) occur within the grain, predominantly around its margins. Unaltered albite exsolution lamellae, oriented E-W, occur in the interior of the grain (not visible at this magnification). The narrow dark lines within patches of pure replacive albite superficially resemble twin composition planes but in fact are trains of micropores that mark the former position of albite films (see Fig. 3). (**b**) Light micrograph (crossed polarizers) of the margin of an alkali feldspar phenocryst. All the albite films in this microperthite (oriented N-S) have thickened, and many are micropore-rich. Small patches of pure replacive albite (PRA) have formed by coalescence of adjacent thickened films. (**c**) SE image of a HF acid etched (001) cleavage surface of a phenocryst. In this field of view are three thickened lamellae (oriented N-S). The lamella on the right side of the image changes from a pristine albite film with paired etch pits at the top to a progressively larger thickened film with euhedral outgrowths of albite toward the middle and lower end of the image. Note the rectangular shape of some outgrowths (arrowed). Between the films is a fine cryptoperthite (coherent albite platelets in tweed orthoclase, CP) of bulk composition $\sim Or_{85}$. (**d**) SE image of a HF acid etched (001) cleavage surface of a phenocryst. A pristine albite film, characterized by sub-regularly spaced pairs of etch pits, occurs along the right hand side of the image. Some of the etch pit pairs along narrow regions of the lamella (bottom right) have coalesced to form a single rectangular pit. The albite lamella in the center of the image has thickened considerably. The interface between albite and enclosing orthoclase is delineated by continuous narrow channels which are inferred to have formed by the coalescence during etching of many closely spaced dislocation etch pits.

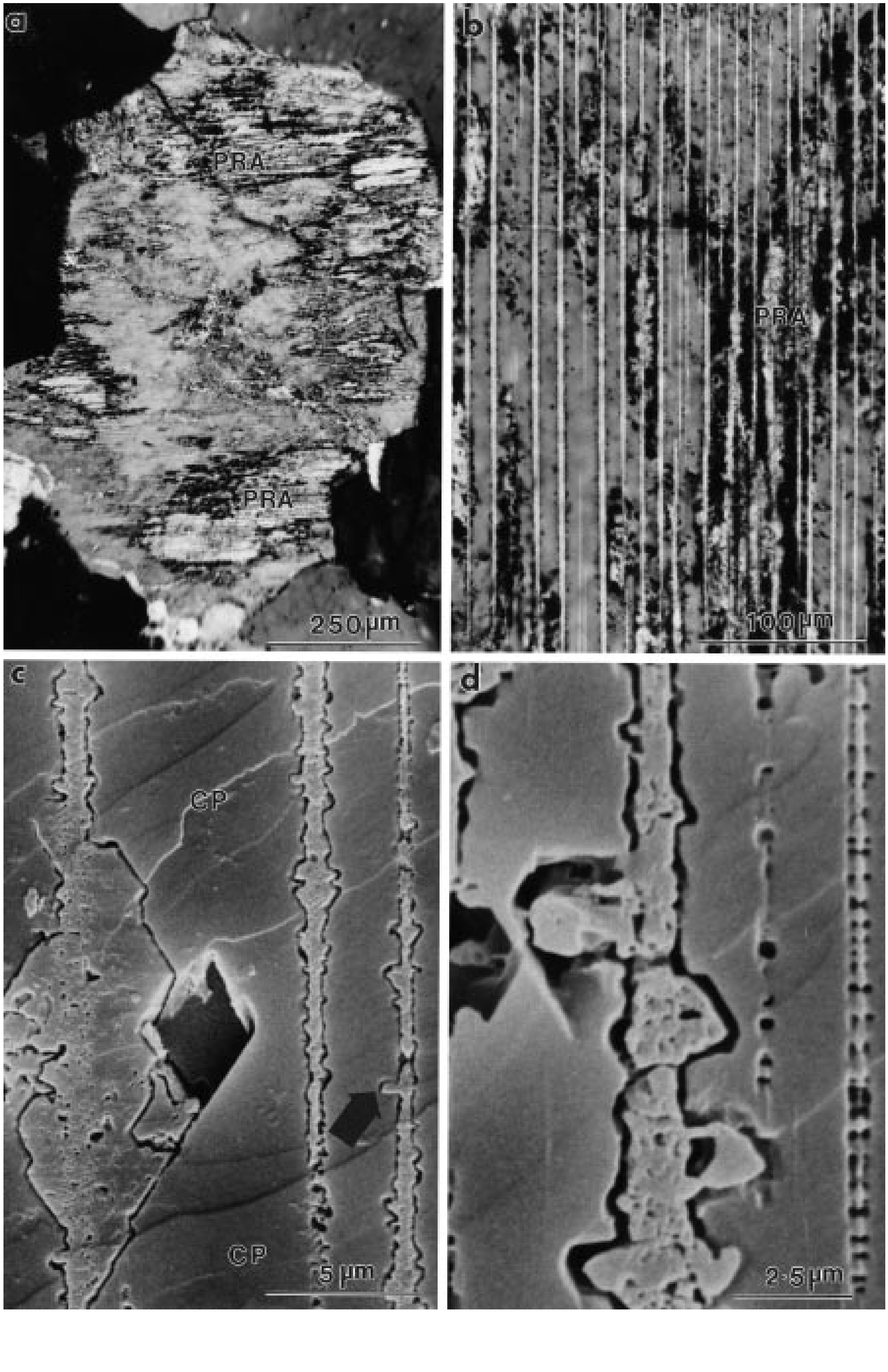
a
PRA
PRA
250 μm
b
PRA
100 μm
c
CP
CP
5 μm
d
2·5 μm

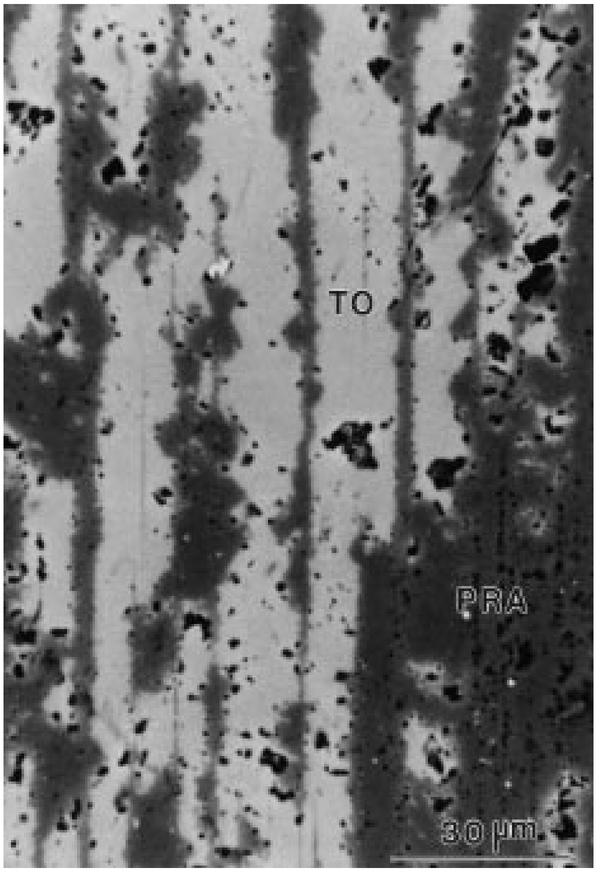

FIGURE 3. BSE image (obtained by SEM) of the margin of a phenocryst showing volumes of pure replacive albite (dark grey, PRA) and thickened lamellae (oriented N–S in the micrograph). Pure replacive albite is characterized by trains of micropores in the same orientation as albite lamellae. Between thickened lamellae is tweed orthoclase (light grey, TO), some of which has been altered to micropore-rich irregular microcline.

Shap phenocrysts, two formed by exsolution (coherent platelets and semicoherent films) and one by deuteric alteration (semicoherent-incoherent patch perthite). Below, we describe a fourth variety of albite-rich feldspar and a second variety of replacive albite that has formed by alteration, that occurs exclusively within alkali feldspar phenocrysts and groundmass crystals, and is characterized by its compositional purity ($Ab_{>99}$, Table 2). Distinguishing features of this pure replacive albite are summarized in Table 1.

DESCRIPTION OF PURE REPLACIVE ALBITE

Light microscopy

Pure replacive albite is most obvious where it forms <500 μm sized rectangular-shaped areas that are turbid and apparently untwinned (Fig. 2a). This albite occurs throughout groundmass crystals (Fig. 2a) but is seen only within ~700 μm of the margins of phenocrysts (Fig. 2b), where it is particularly abundant around inclusions of biotite and quartz. The boundary between pristine film microperthite in phenocryst interiors and volumes of pure replacive albite around their margins is gradational and occurs by a gradual thickening and eventual coalescence of albite films. Thickened films are distinguished from pristine ones by their greater width and particularly by the abundance of micropores and fluid inclusions along their length (Fig. 2b). Most albite films within ~1 mm of the margins of phenocrysts are thickened, but only those in the immediate vicinity of grain boundaries have coalesced to produce volumes of pure albite (Figs. 2a and 2b). The majority of albite films in groundmass alkali feldspars have also thickened, thus precluding any determination of the bulk chemical composition of pristine microperthite in these grains. The cryptoperthitic rims on phenocrysts and groundmass crystals have escaped replacement by pure albite.

Secondary and backscattered electron microscopy

SE images of HF acid-etched cleavage surfaces show the progressive nature of thickening of albite films (Figs 2c and 2d). Initially, submicrometer-sized, rectangular crystals of albite project from otherwise pristine films into orthoclase. Many of these albite projections occur in pairs straddling the films and their margins are oriented parallel to $\{020\}_{\text{orthoclase}}$. As these albite projections increase in size, their margins rotate to parallel to $\{130\}_{\text{orthoclase}}$ and maintain this same crystallographically defined shape until they

→

FIGURE 4. Bright-field TEM images of partially albitized and thickened semicoherent albite films in tweed orthoclase, from a groundmass alkali feldspar. Electron beam near [001]. (**a**) A semicoherent albite film (oriented NW–SE) showing the earliest stages of replacement. The main body of the film is pericline twinned but has been partially replaced by four small crystals of albite-twinned albite (A). The occurrence of these replacive crystals, in pairs straddling the lamella, indicates that alteration was specific to areas of strain around pairs of edge dislocations. (**b**) A pericline-twinned semicoherent albite film (oriented E–W) which is straddled by two pairs of edge dislocations. Albite and orthoclase surrounding three of the four dislocations (D) is largely, although not completely unaltered. A crystal of albite (A) has selectively replaced highly strained orthoclase surrounding one of the dislocations. The interface of this replacive albite crystal with orthoclase is delineated by numerous alternating strain shadows probably related to closely spaced dislocations. (**c**) A mainly albite-twinned semicoherent albite film (oriented NW-SE) containing numerous euhedral outgrowths of albite. Note how most outgrowths occur in pairs straddling the film. (**d**) A euhedral outgrowth of albite-twinned albite (A) on a partially altered semicoherent albite film (oriented NW-SE). Note the alternating strain shadows along the (010)-parallel interface between the albite outgrowth and orthoclase, which are spaced ~12–15 nm apart. This outgrowth is very similar in size and shape to those seen on HF acid etched surfaces (see Fig. 2c).

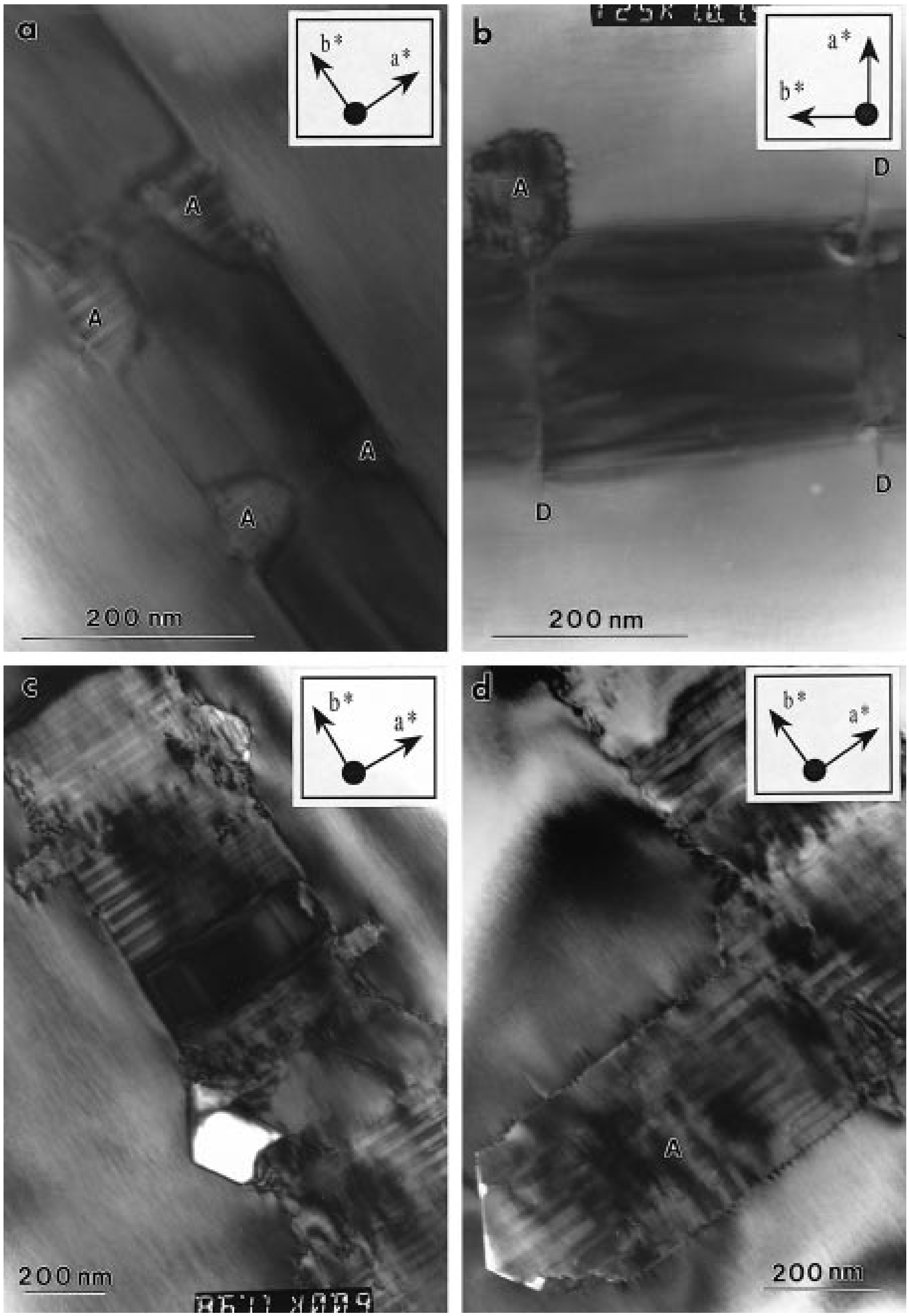
a
b*
a*
A
A
A
A
200 nm
b
a*
b*
A
D
D
D
200 nm
c
b*
a*
200 nm
d
b*
a*
A
200 nm

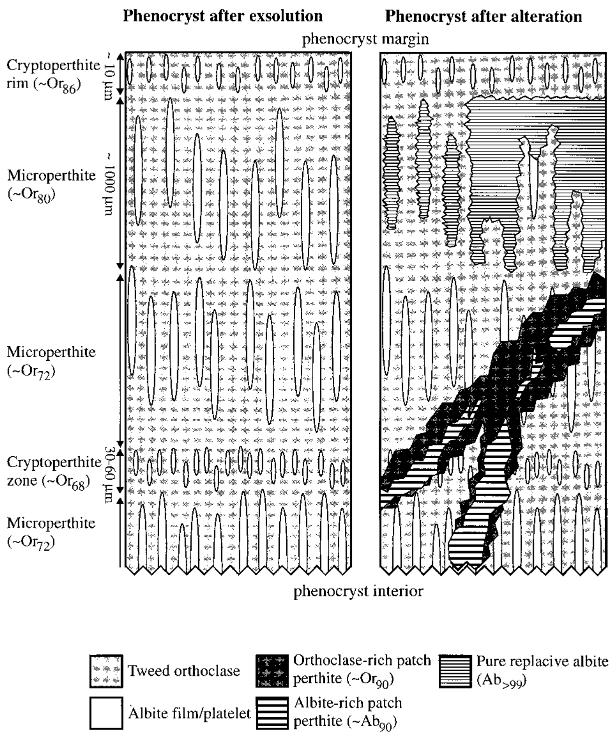

FIGURE 5. Schematic diagram of the margin of a Shap phenocryst in the plane (001) before and after both stages of alteration. The diagram illustrates the spatial relationships between pristine exsolution microtextures and volumes of replacive feldspar. Pure replacive albite has selectively replaced microperthites within ~1 mm of the margins of phenocrysts whereas anastomosing veins of albite and irregular microcline cut across microtextures throughout the interior of phenocrysts.

eventually meet across intervening orthoclase. Continuous narrow channels, which delineate the interface of albite outgrowths into orthoclase (Fig. 2d), are inferred to have formed by the coalescence of many closely spaced dislocation etch pits. Ghostlike relics of original semicoherent albite lamellae extend across areas of coarse replacive albite (Fig. 2c, bottom right).

The micropores that give volumes of pure replacive albite their turbid appearance in light microscopy are ~0.5–4.0 μm in size and usually occur in parallel trains that are spaced a few micrometers apart (Fig. 3). The orientation and spacing of these micropore trains indicates that they represent the former location of albite films. Thickened films adjacent to volumes of pure albite are ~1.0–2.5 μm in width and spaced an average of ~5 μm apart (Fig. 3). The interface of thickened films with orthoclase is delineated by euhedral outgrowths of albite often associated with micropores (Fig. 3).

Transmission electron microscopy

TEM images reveal the earliest stages in the formation of thickened lamellae (Fig. 4). Pure albite initially replaces the semicoherent albite films in the immediate vicinity of edge dislocations, producing nearly regularly spaced pairs of ~100 nm sized crystals of albite-twinned albite (Figs 4a, b). These crystals are most obvious where they have replaced pericline-twinned albite films (pericline twin composition planes cannot be imaged when looking down [001]) (Fig. 4a). From these initial sites of replacement, pure albite expands further into the semicoherent albite film, where it is frequently associated with micropores, or into tweed orthoclase (Figs. 4b, c, d), producing the euhedral projections of albite that were seen on HF acid-etched surfaces (Figs. 2c, d). The interfaces of rectangular grains of pure albite with orthoclase parallel to (010) are incoherent or semicoherent; alternating strain shadows occur every ~12–15 nm along the interface (Fig. 4d), which may reflect the periodicity of dislocations. The difference in 200 lattice spacings of low albite (d_{200} = 0.3639 nm) and low sanidine (d_{200} = 0.3847 nm) at room temperature is 5.5%. If both minerals have no homogeneous strain one dislocation should occur every 6.73 nm along (010) parallel grain boundaries. This is exactly half the repeat distance of the strain shadows, perhaps suggesting that each strain shadow is the product of two dislocations and that the pure replacive albite has no homogeneous strain. Strain is restricted to the interface, between dislocations, rising to a maximum at the dislocation. It seems to us remarkable that the replacement process can lead to a semicoherent interface of this type. It implies that at the temperature when replacement occurred, a semicoherent interface with homogeneous strain and dislocations made a smaller contribution to the Gibbs free energy than did the surface energy of a fully incoherent interface.

Electron probe analysis

Compositions of pure replacive albite in phenocrysts and groundmass crystals are the same. The small standard deviations of their average bulk-molecular compositions demonstrate their homogeneity (Table 2). During electron probe analysis, pure replacive albite luminesces very dull orange. The microperthites around phenocryst margins, which contain abundant thickened lamellae (Fig. 2b), have a comparable mean bulk composition to pristine microperthites in phenocryst interiors ($Or_{72.4}$ and $Or_{71.8}$, respectively). As these marginal microperthites have had extensive addition of albite to form the thickened lamellae, before alteration they must have been considerably more orthoclase-rich than pristine microperthites in phenocryst interiors. Volumes of pristine orthoclase-rich feldspar between individual thickened lamellae have an average bulk composition of ~Or_{85}, which is comparable to the cryptoperthite rims and indicates that this orthoclase-rich feldspar is itself a cryptoperthite (Table 2). Taking into account the average width and spacing of still-pristine semicoherent albite films in marginal microperthites (~0.25 μm and ~5.0 μm, respectively; Fig. 2d), the marginal microperthites would have had a bulk composition of ~Or_{80} before thickening. The micro-

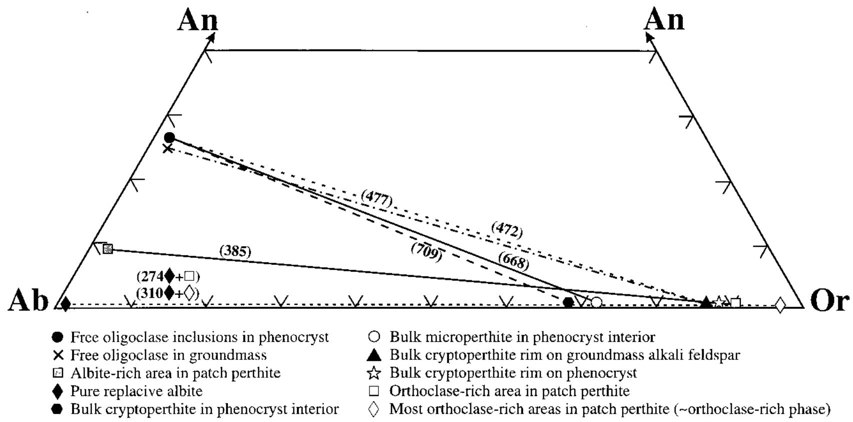

FIGURE 6. Ternary diagram illustrating the composition of various feldspar phases within alkali feldspar crystals in the Shap granite. Average compositions were taken from Table 2. Various tie-lines are shown, with temperatures (°C) calculated using the two-feldspar geothermometer of Fuhrman and Lindsley (1988) assuming a pressure of 0.1 GPa. Note that these temperatures are for feldspars with disordered Si-Al-O frameworks. Estimates for ordered pairs are given in Table 3.

textures of Shap granite phenocrysts before and after alteration are illustrated in Figure 5.

DISCUSSION

Previous descriptions of pure replacive albite

Several authors have noted a narrow "white border," "white marginal zone," or "albitic margin" to some alkali feldspar phenocrysts and groundmass crystals from the Shap granite (Harker and Marr 1891; Grantham 1928; Firman 1978; Caunt 1986). Harker and Marr (1891) inferred this white border to be made of plagioclase and suggested that its formation was by "corrosive alteration rather than an original intergrowth."

Compositionally pure replacive albite has been described from the Beinn an Dubhaich granite on Skye by Ferry (1985) and from the Siljan granite, Sweden by AlDahan et al. (1987) and Ramseyer et al. (1992). The albite described by Ferry (1985) had a composition of $Ab_{99}Or_1$ and was interpreted to have formed at 350–400 °C during hydrothermal alteration. Pure albite in the Siljan granite ($Or_{0.2}Ab_{99.5}An_{0.3}$), which formed by replacement of microcline during low grade metamorphism, is untwinned, inclusion-rich, and luminesces dark brown. Albitization was progressive, by the coalescence of albite films that had formed along cleavages, and is inferred to have taken place at ~200–300 °C (AlDahan et al. 1987).

Distinctive microtextures consisting of crystals of replacive albite around alkali feldspar grain boundaries occur in hypersolvus granites and syenites. These swapped rims are seen only where two alkali feldspar grains are in contact (Voll 1960; Parsons 1965) and form by fluid-induced grain boundary migration of albite from one crystal to the adjacent crystal. The newly formed albite has the same crystallographic orientation as albite in its parent crystal. These microtextures are however significantly different from pure replacive albite in the Shap granite; swapped rims are not micropore-rich, and pure replacive albite in the Shap granite does not occur only where two alkali feldspar grains are in contact.

Chemical relationships of feldspars and temperature of albitization

Compositions of the feldspars in the Shap granite are plotted on Figure 6 together with tie-lines for feldspar pairs which were or are, on textural grounds, possibly (see below) in equilibrium. A surprising result is that the anorthite content of the albite-rich phase in patch perthite veins in the phenocrysts (Fig. 1) is too high for it to have formed as a result of isochemical coarsening of the regular crypto- and microperthitic intergrowths that surround it. For isochemical coarsening to be possible the albite- and orthoclase-rich parts of the patch perthite would have to lie on a tie-line passing through the bulk composition of the regular intergrowths, and they clearly do not. Thus the patch perthites must, to some degree, be replacive, with relative addition of anorthite. The most probable source of this component is the oligoclase in the groundmass or the free oligoclase included in the phenocryst. We have not, however, encountered any direct textural evidence that this phase is participating in the coarsening reaction.

Provided pressure is known, the ternary compositions of feldspar pairs can be used to calculate the temperature at which they reached equilibrium. Many two-feldspar geothermometers exist for estimating the temperature at which pairs of feldspars with disordered Si-Al-O frameworks were in equilibrium. However, as is usually the case in alkali feldspars from subsolvus granites and as Table 2 illustrates, bulk compositions and individual phase compositions in the Shap alkali feldspars vary from point-to-point within individual crystals. It is by no means straightforward to deduce which pairs of feldspar phases, if any, are or were in exchange equilibrium with respect to the three feldspar components, orthoclase, al-

TABLE 3. Temperatures (°C) for coexisting feldspar pairs calculated using the Fuhrman and Lindsley (1988) two-feldspar geothermometer

	Alkali feldspar	Or	Ab	An	Plagioclase	Or	Ab	An	T_{Or}	T_{Ab}	T_{An}	T_{Dis}	T_{Ord}
1	Phenocryst: bulk interior cryptoperthite	68.0	31.1	0.8	Free oligoclase inclusions	1.7	71.8	26.5	629	725	692	709	810
2	Phenocryst: bulk microperthite	71.8	27.6	0.6	Free oligoclase inclusions	1.7	71.8	26.5	624	690	646	668	770
3	*Phenocryst: bulk rim thickened microperthite*	*72.4*	27.1	*0.5*	Groundmass oligoclase	2.3	72.9	24.8	*674*	*639*	*648*	*654*	*750*
4	Beginning of coherent exsolution in phenocryst cryptoperthite	68.0	31.1	0.8									670
5	Phenocryst: bulk rim cryptoperthite	85.9	13.9	0.2	Groundmass oligoclase	2.3	72.9	24.8	477	477	476	477	580
6	Groundmass: bulk cryptoperthite rim	85.5	14.4	0.2	Groundmass oligoclase	2.3	72.9	24.8	477	477	476	477	580
7	Phenocryst: bulk rim cryptoperthite	85.9	13.9	0.2	Free oligoclase inclusions	1.7	71.8	26.5	475	471	471	472	570
8	Beginning of coherent exsolution in groundmass cryptoperthite	85.5	14.4	0.2									
9	*Orthoclase-rich areas in patch perthite*	*90.4*	*9.4*	*0.3*	*Albite-rich areas in patch perthite*	*1.5*	*89.8*	*8.7*	*400*	*369*	*460*	*385*	*490*
10	*Orthoclase-rich areas in patch perthite*	*90.4*	*9.4*	*0.3*	Pure replacive albite	0.7	99.1	0.2	*277* [*271*]	*343* [*333*]	*846* [*853*]	*310* [*302*]	*410* [*400*]
11	Most orthoclase-rich analysis in patch perthite areas	96.2	3.7	0.1	Pure replacive albite	0.7	99.1	0.2	274 [267]	274 [264]	1139 [1146]	274 [266]	370 [370]

Notes: Items in italics are probably not bulk compositions of phases that were homogeneous at any T and the calculated T and are not reliable. All T were calculated for 0.1 GPa except those in square brackets which are for atmospheric pressure. Analytical detail is in Table 1. T_{Dis} is the best estimate of the equilibrium T (for disordered feldspars) extracted from the T for the three components, using the criteria suggested by Fuhrman and Lindsley (1988). T_{Ord} is the approximate equivalent T for ordered frameworks using the T correction suggested by Brown and Parsons (1989). T_{Ord} in rows 4 and 8 is estimated from Figure 8b in Brown and Parsons (1989) with adjustment for anorthite.

bite, and anorthite. Strictly, at complete equilibrium, the rock can contain a maximum of two feldspar phases at any temperature. In practice, the rock contains at least three compositionally distinct generations of plagioclase. Each of these may have been in equilibrium with one of at least four alkali feldspars, each of which has subsequently unmixed to produce two further feldspar phases in perthitic intergrowth. In addition, the orthoclase-rich and albite-rich areas in the patch perthite (Fig. 1) are not single phases but on the microscale contain subgrains of the alternate phase. The areas of phenocryst rims with thickened albite lamellae, and areas in which albite lamellae have been replaced by microcline, have bulk compositions that clearly have been modified subsequent to any stage at which the original bulk feldspar was in equilibrium with a plagioclase. Thus, application of a geothermometer to pairs of feldspars analyzed by electron probe, without taking account of texture, is certain to be meaningless. A further complication arises because of Si-Al ordering: in our present assemblage the phases are, at surface temperature, low albite (~fully ordered) with low microcline (~fully ordered) or tweed orthoclase (less than fully ordered), but at magmatic temperature, the crystals probably had a considerable degree of framework disorder (see Brown and Parsons 1989, Fig.7).

Lee et al. (1995) applied two-feldspar geothermometers to the Shap feldspars to reveal magmatic growth conditions. We used the program SOLVCALC (provided by H. Nekvasil and S. Wen, State University of New York, Stony Brook) to find thermometers that gave temperatures in best agreement, with the experimentally reversed binary albite-orthoclase solvus of Smith and Parsons (1974). The thermometers of Elkins and Grove (1990) and Fuhrman and Lindsley (1988) gave best agreement, and the Fuhrman-Lindsley thermometer was used to obtain estimates of temperature in the present work. We assumed a pressure of 0.1 GPa, which is geologically reasonable for the emplacement of the Shap granite. It is possible that the albitization described here occurred at lower pressure, but the effect of pressure is small and results in a lowering of temperature by ~10 °C for atmospheric pressure. The effect of Si-Al ordering is not well known, particularly at low temperature, but for reasons given in Brown and Parsons (1989) calculated temperature should be increased by ~100 °C, for fully ordered feldspar pairs.

Various temperatures calculated from the Fuhrman-Lindsley thermometer are given in Table 3. Their approach allows the calculation of three temperatures T_{Ab}, T_{Or}, and T_{An} based on the equilibrium partitioning of each component (albite, orthoclase, and anorthite) between the two phases alkali feldspar (AF) and plagioclase (PL) such that the activities (a) are equalized: $a^{AF}_{Ab} = a^{PL}_{Ab}$, $a^{AF}_{Or} = a^{PL}_{Or}$, and $a^{AF}_{An} = a^{PL}_{An}$. Fuhrman and Lindsley considered that equilibrium feldspar pairs should generate three temperature estimates within 40 °C of each other, and close-to-equilibrium pairs should provide two concordant (within 40 °C) and one discordant apparent temperatures (≤100 °C different). When the three temperature estimates differ by >40 °C, T_{Ab} is likely to be closest to equilibrium because it depends on the slope of the alkali feldspar-plagioclase tie-line in the albite-orthoclase-anorthite ternary system, while small measurement errors in X^{AF}_{An} and X^{PL}_{Or} (both small at low temperature), can lead to significant errors in T_{An} and T_{Or}. Where there is doubt as to which pairs in a complex feldspar assemblage are in equilibrium, the concordance of the calculated temperatures can provide some guidance, although, as we show below, in the absence of microtextural information, this can be misleading. Fuhrman and Lindsley's criteria have been used in Table 3 to provide the best estimates of temperature in the right columns.

The temperatures in rows one and two of Table 3 provide estimates of the temperature of magmatic growth of the alkali feldspar phenocrysts in Shap, which grew as homogeneous sanidine possibly in equilibrium with free (non-perthitic) oligoclase inclusions. T_{Ab} and T_{An} are concordant and the estimates obtained from bulk crypto- and bulk microperthite from the interior of the phenocrysts do not differ significantly, suggesting growth at 690 °C (if fully disordered) and ~790 °C (if fully ordered). These estimates are similar to those provided by Lee et al. (1995), but are based on more analyses. We expect the bulk cryptoperthite to provide the best estimate of magmatic temperature, and these estimates are in good agreement with solidus temperature for similar rocks at 0.1 GPa (Nekvasil 1988). Row three in Table 3 provides an example of a reasonable but texturally unsupportable temperature; we showed above that the thickened microperthite in the initially cryptoperthitic rims formed by adding albite to the bulk cryptoperthite in row five, not by isochemical coarsening.

Row four in Table 3 provides an estimate of the maximum temperature at which coherent exsolution of the phenocrysts, leading to cryptoperthite, could have occurred, estimated from Figure 8b in Brown and Parsons (1989). The fine lamellar cryptoperthites would begin to form after the cooling crystals intersected the coherent solvus but before they intersected the coherent spinodal (see Lee et al. 1995). For anorthite-free low sanidine, with bulk composition Or_{68}, (equivalent to the phenocryst interiors, row one in Table 3) the coherent solvus for ordered crystals is at ~520 °C. The anorthite-content (~0.8%) will increase coherent exsolution temperature by >150 °C (Lee et al. 1995), suggesting a maximum temperature for the beginning of coherent exsolution of ~670 °C. The cryptoperthite rimming the phenocrysts (row eight), and that in the groundmass, is more orthoclase-rich (Or_{86}) and anorthite-poor ($An_{0.2}$), and will have begun to exsolve coherently below ~360 °C, ignoring anorthite, or 410 °C if 50 °C is added for the effect of anorthite. On textural grounds this phase of exsolution preceded the formation of patch perthite.

Rows five to seven in Table 3 provide estimates for the crystallization of the groundmass of the granite (both AF and PL in the groundmass) and for the final stage of crystallization (the rim) of the phenocrysts assumed to be growing simultaneously with either the free oligoclase inclusions or the groundmass oligoclase. These T_{Dis} estimates are highly concordant, all within 4 °C of an average of 475 °C, suggesting a close approach to exchange equilibrium at ~580 °C if ordered. The bulk groundmass AF is more orthoclase-rich than the bulk phenocryst AF as predicted by phase-equilibria if the liquid composition changes little during crystallization (Nekvasil 1992, Fig. 2). However temperatures are too low (by at least 200 °C at P_{H_2O} 0.1 GPa) for the crystals to have reached exchange equilibrium in the presence of melt. This might be explained in three ways. (1) Exchange of feldspar components between the feldspar phases continued (in the fine-grained groundmass and in the phenocryst rims) below solidus temperature. (2) Crystals reached equilibrium when they had a high degree of Si-Al order. (3) The feldspars grew in exchange equilibrium with each other but at a high degree of undercooling. The most probable explanation is a combination of (1) and (2); T_{Dis} of 475 °C, therefore, is not significant but reflects the kinetics of exchange during cooling.

For the albite-rich and orthoclase-rich areas of patch perthite (row nine), two-feldspar temperatures (385 to 485 °C, depending on the degree of order) are higher than the beginning of exsolution in the groundmass cryptoperthite (row eight) which seems unlikely. However, on the micro-scale the albite-rich and orthoclase-rich areas in patch perthite are not individual phases but are areas in which albite or orthoclase phases are concentrated, so although T_{Ab} and T_{Or} appear reasonably concordant this is not necessarily a meaningful temperature. Finally, the pure replacive albite might, in principle, be in equilibrium with the most albite- and anorthite-poor orthoclase-rich patches in patch perthite. The Fuhrman and Lindsley thermometer gives (row eleven) T_{Dis} of 274 °C with perfect concordance for T_{Ab} and T_{Or} suggesting T_{Ord} of <370 °C although these low temperatures represent a long extrapolation of the experimental work used to construct the thermometer, and the effect of ordering is poorly known. However, the estimate is in good agreement with Figure 8a in Brown and Parsons (1989) which can be applied because anorthite is negligible in both phases.

Although the accuracy of the low temperature estimates using these geothermometers may be low, because of the poorly known effects of ordering and anorthite content, the general evolution of the microtextures with decreasing temperature is in line with deductions on textural grounds, and the relative changes in temperature are reasonably robust. The feldspar assemblage provides a record of events extending from the magma solidus to near-surface temperature. Note that low albite in equilibrium with potassium feldspar is essentially pure below 400 °C (Brown and Parsons 1989, Fig. 8a) so that the range of temperature for albitization in late-stage igneous and sedimentary environments overlaps and is poorly defined by the composition of the albite.

Driving forces for albitization in the Shap granite

The restriction of pure replacive albite to specific areas of grains may help determine which factors controlled its distribution. Pure albite occurs throughout small groundmass alkali feldspars but only within ~1 mm of the margins of phenocrysts and it has replaced microperthites, although cryptoperthite zones and rims have been unaffected. The restriction of pure replacive albite to grain boundaries suggests that albitization was mediated by a fluid and that this fluid was derived from the groundmass of the granite. As the bulk composition of the alkali feldspar has changed, K-Na interchange on a large scale, perhaps intrusion-wide, provided a chemical driving force for replacement. However, selective replacement of microperthites demonstrates that exsolution microtexture, and in particular the size and coherency of exsolution lamellae controlled the manner in which these grain boundary fluids interacted with the feldspars.

On a grain-scale, albitization is inferred to have been driven by reductions in Gibbs free energy resulting from replacement of elastically strained microperthites by unstrained albite (termed unzipping by Brown and Parsons 1989). This control is most vividly illustrated by the initial stages of albitization in which compositionally pure semicoherent albite films were replaced by compositionally pure albite (Fig. 4a); there is clearly no local chemical driving force for this low albite to low albite replacement reaction. This earliest formed replacive albite occurs in the immediate vicinity of edge dislocations on semicoherent albite films. These regions have the highest elastic strain within pristine microperthites and therefore the greatest thermodynamic driving force for replacement. Once the fluid had gained access to highly elastically strained albite around a dislocation, for example by means of a fracture or open cleavage plane, alteration of entire films was facilitated by the three dimensional interconnectivity of edge dislocations over their surfaces. After the most highly strained albite had been replaced, pure albite continued to grow into the homogeneously and less highly elastically strained albite between dislocations.

Albitization of tweed orthoclase, which produced the thickened lamellae, is also inferred to have been partly driven by reductions in strain energy. Replacement by unstrained pure albite releases strain energy in domain walls and further reductions in Gibbs free energy come from coarsening of the tweed microtexture. These thermodynamic gains are partially opposed, however, by the positive contribution to free energy resulting from formation of semicoherent subgrain boundaries. Although total elastic strain energy per mole decreases as a result of albitization of a given volume of orthoclase, formation of micropores and noncoherent subgrains may have the effect of increasing the susceptibility of partially albitized orthoclase to subsequent fluid-feldspar interaction. This is because there is a greater thermodynamic drive for replacement of highly elastically strained feldspar around the newly formed dislocations than unstrained pure albite or homogeneously and less highly strained orthoclase. The interconnectivity of micropores associated with replacive albite subgrains will also facilitate fluid ingress into grain interiors (Walker 1990). Thus, once semicoherent albite films have been transformed to incoherent films by initial thickening, complete albitization of microperthites may proceed rapidly. The factor that limited the albitization of Shap granite alkali feldspars is likely to be the volume of Na-rich intergranular fluid available instead of the thermodynamic driving force for replacement.

Composition and origin of the grain boundary fluid

That partially albitized phenocrysts and groundmass alkali feldspars have changed significantly in bulk chemical composition shows that the alteration reaction was open with respect to major elements at the scale of a rock sample. Deuteric alteration sensu stricto is closed with respect to major elements at the scale of an intrusion, although trace elements and isotopes may be exchanged. Possibly the fluids that mediated albitization of Shap granite alkali feldspars were predominantly magmatic in origin but gained Na from sericitization of free oligoclase. Such a hypothesis is consistent with the highly sericitized nature of free oligoclase in the Shap granite and AlDahan et al. (1987) have also suggested that Na for pure replacive albite in the Siljan granite was derived from sericitization of free plagioclase. Alternatively, albitization may have taken place during relatively high-temperature fluid-rock interaction; the Shap granite is surrounded by a ~1 km wide metamorphic aureole within which fissure metasomatism has taken place and sulfides occur in both the granite and its aureole (Harker and Marr 1891, 1893; Firman 1957; O'Brien et al. 1985). Formation of pure replacive albite during large scale metasomatism is however unlikely, given the low temperature at which it is inferred to have crystallized. Thus the fluid source from which pure replacive albite formed cannot be determined with certainty, but was probably modified magmatic or low-temperature hydrothermal fluid. Note that the work of Orville (1963) showed that the fluid does not need to be Na-rich. It merely has to provide a medium for exchange of Na^+ and K^+ in a temperature gradient in which Na migrates to the hotter end of a system containing two feldspars at both hot and cold ends.

Constraints on the temperature of formation of edge dislocations

Patch perthite albite veins clearly formed earlier and at higher temperature than the pure replacive albite. The radiation of some albite veins away from inter- and intragranular boundaries indicates that the deuteric fluids were derived from outside phenocrysts. Once the process of dissolution and reprecipitation had begun inside the crystals, exsolution microtextures appear to have exerted little control on the paths of fluid movement and interaction because the albite and microcline veins crosscut microperthites and penetrate into the cores of grains on the scale of tens of millimeters. Such a distribution of replacive feldspar indicates that elastic strain energy, whose release was the main driving force for this phase of alteration, was relatively homogeneously distributed at this temperature, and dislocations had not formed. There were no thermodynamic and kinetic advantages in the alteration of specific microtextures (i.e., semicoherent albite films). As the granite continued to cool however, the strain at exsolution interfaces would have progressively increased as albite and orthoclase would have become elastically stiffer and their unit-cell parameters differed more and more; dislocations would have formed along albite films once local elastic strain had exceeded a threshold value.

Differences in microtextural control of the two episodes of alteration in phenocrysts enable an estimation of the temperature at which most edge dislocations on albite films developed. We can conclude, from Table 3 row eleven, that the dislocations had formed by the time the feldspars had cooled to 370 °C. It seems improbable that patch perthite in the phenocrysts could form before the beginning of exsolution in the groundmass cryptoperthite, because fluid-feldspar reactions affecting the phenocrysts could inevitably affect the groundmass. Thus the development of most of the dislocations can be placed between 410 °C (Table 3, row eight) and 370 °C (row eleven).

Diagenetic albitization of detrital alkali feldspars

Diagenetic replacive albite in siliciclastic sedimentary rocks has several characteristic chemical and petrographic features: (1) compositional purity ($Ab_{>98-99}$), (2) cloudy or vacuolised appearance in thin section, (3) absence of twinning or chessboard twinning, and (4) lack of cathodoluminescence (Kastner 1971; Walker 1984; Saigal et al. 1988). Replacive albite in the Shap and Siljan granites is compositionally pure, cloudy, untwinned (at the scale of light microscopy) and has dark luminescence colors. We do not doubt that albitization can be a common diagenetic process in some siliciclastic sedimentary rocks; trends of increasing volumes of replacive albite with depth through thick sedimentary sequences (Saigal et al. 1988) clearly demonstrate its importance. However, our results do show that care must be taken when determining the origin of replacive albite in detrital alkali feldspars from clastic sedimentary rocks; formation by deuteric-hydrothermal alteration in the igneous protoliths of feldspar grains should be considered as a possible origin.

The compositional and petrographic similarities between pure replacive albite in granites and siliciclastic sedimentary rocks suggests that the replacement reactions may be comparable in these two geological environments. The nearly pure chemical composition indicates replacement at similarly low temperature in both contexts. From examination of deep borehole cores of Mesozoic and Tertiary sedimentary rocks in the North Sea, Saigal et al. (1988) showed that albitization of potassium feldspar starts at ~65 °C and reaches a maximum at ~105 °C. The apparent absence of twinning in the Shap albite is because constituent crystals are very small and so their albite twins, which have a submicrometer periodicity, cannot be resolved by light microscopy. The same conclusion was reached for the apparent lack of twinning in pure replacive albite from the Siljan granite (AlDahan et al. 1987). Diagenetic albite, which appears frequently to be untwinned, possibly consists of many suboptically twinned subgrains. The cloudy appearance of replacive albite in the Shap granite is due to the presence of micropores, which are a fingerprint of deuteric alteration and result from a small net loss of feldspar during alteration (Walker et al. 1995). Diagenetic albitization may also be associated with a small volume decrease. An important implication of the apparent similarities between deuteric or hydrothermal and diagenetic albitization is that the relaxation of elastic strain energy may also be a major driving force for diagenetic alteration of feldspars. As a result, the microtexture of a detrital alkali feldspar when it enters a clastic sedimentary rock (e.g., coherent vs. semicoherent) may have a considerable influence on its subsequent diagenetic history.

Acknowledgments

We thank David Hulmes (Department of Biochemistry, University of Edinburgh) and Chris Jeffree (Department of Botany, University of Edinburgh) for provision of TEM and SEM facilities and Pete Hill and Stuart Kearns (Department of Geology and Geophysics) for assistance with electron probe analyses. An earlier version of this manuscript was improved considerably by constructive reviews from David C. Elbert and Kathryn L. Nagy. This work was supported by research grants from NERC (GR3/8374 and GR3/10290)

References cited

AlDahan, A.A., Morad, S., and Collini, B. (1987) Clouded-untwinned albite in the Siljan granite, central Sweden. Neues Jahrbuch Fur Mineralogie-Monatshefte, 327–335.

Brown, W.L. and Parsons, I. (1989) Alkali feldspars: ordering rates, phase transformations and behaviour diagrams for igneous rocks. Mineralogical Magazine, 53, 25–42.

——— (1993) Stored elastic strain energy: the driving force for low-temperature reactivity and alteration of alkali feldspar. In J. Boland and J.D. Fitz Gerald, Eds., Defects and Processes in the Solid State: Geoscience Applications. The McLaren Volume, p. 267–290, Elsevier, Amsterdam.

——— (1994) Feldspars in igneous rocks: In I. Parsons, Ed., Feldspars and their reactions, NATO ASI 421, p. 449–499, Kluwer, The Netherlands.

Brown, W.L., Becker, S.M., and Parsons, I. (1983) Cryptoperthites and cooling rate in a layered syenite pluton: a chemical and TEM study. Contributions to Mineralogy and Petrology, 82, 13–25.

Caunt, S.L. (1986) Igneous and metamorphic processes in the Shap granite and its aureole. Unpublished Ph.D. thesis, University of Leeds.

Cox, R.A., Dempster, T.J., Bell, B.R., and Rogers, G. (1996) Crystallization of the Shap granite: evidence from zoned K-feldspar megacrysts. Journal of the Geological Society, London, 153, 625–635.

Grantham, D.R. (1928) The petrology of the Shap granite. Proceedings of the Geological Association, 39, 299–331.

Eggleton, R.A. and Buseck, P. R. (1980) High resolution electron microscopy of feldspar weathering. Clays and Clay Minerals, 28, 173–8.

Elkins, L.T. and Grove, T.L. (1990) Ternary feldspar experiments and thermodynamic models. American Mineralogist, 75, 544–559.

Ferry, J.M. (1985) Hydrothermal alteration of Tertiary igneous rocks from the Isle of Skye, northwest Scotland II. Granites. Contributions to Mineralogy and Petrology, 91, 283–304.

Firman, R.J. (1957) Fissure metasomatism in volcanic rocks adjacent to the Shap granite, Westmorland. Quarterly Journal of the Geological Society of London, 113, 205–222.

——— (1978) Intrusions. In F. Moseley, Ed., The Geology of the Lake District, p. 146–167, Yorkshire Geological Society, Leeds.

Fuhrman, M.L. and Lindsley, D.H. (1988) Ternary feldspar modelling and thermometry. American Mineralogist, 73, 201–215.

Harker, A. and Marr, J.E. (1891) The Shap granite, and the associated igneous and metamorphic rocks. Quarterly Journal of the Geological Society of London, 47, 266–328.

——— (1893) Supplementary notes on the metamorphic rocks around the Shap granite. Quarterly Journal of the Geological Society of London, 49, 359–371.

Kastner, M. (1971) Authigenic feldspars in carbonate rocks. American Mineralogist, 56, 1403–1442.

Kastner, M. and Siever, R. (1979) Low temperature feldspars in sedimentary rocks. American Journal of Science, 279, 435–479.

Lee, M.R. and Parsons, I. (1995) Microtextural controls on weathering of perthitic alkali feldspars. Geochimica et Cosmochimica Acta, 59, 4465–4488.

——— (1997) Compositional and microtextural zoning in alkali feldspars from the Shap granite and its geochemical implications. Journal of the Geological Society of London, in press.

Lee, M.R., Waldron, K.A., and Parsons, I. (1995) Exsolution and alteration microtextures in alkali feldspar phenocrysts from the Shap granite. Mineralogical Magazine, 59, 63–78.

Lee, M.R., Waldron, K.A., Parsons, I. and Brown, W.L. (1997) Fluid-feldspar interactions in braid microperthites: pleated rims and vein microperthites. Contributions to Mineralogy and Petrology, in press.

Nekvasil, H. (1988) Calculation of equilibrium crystallization paths of compositionally simple hydrous felsic melts. American Mineralogist, 73, 956–965.

——— (1992) Ternary feldspar crystallization in high-temperature felsic magmas. American Mineralogist, 77, 592–604.

O'Brien, C., Plant, J.A., Simpson, P.R., and Tarney, J. (1985) The geochemistry, metasomatism and petrogenesis of the granites of the English Lake District. Journal of the Geological Society of London, 142, 1139–1157.

Orville, P.M. (1963) Alkali ion exchange between vapour and feldspar phases. American Journal of Science, 261, 201–237.

Parsons, I. (1965) The feldspathic syenites of Loch Ailsh intrusion, Assynt, Scotland. Journal of Petrology, 6, 365–394.

——— (1978) Feldspars and fluids in cooling plutons. Mineralogical Magazine, 42, 1–17.

——— (1980) Alkali-feldspar and Fe-Ti oxide exsolution textures as indicators of the distribution of subsolidus effects of magmatic 'water' in the Klokken layered syenite intrusion, South Greenland. Transactions of the Royal Society of Edinburgh, Earth Sciences, 71, 1–12.

Parsons, I., Rex, D.C., Guise, P., and Halliday, A.N. (1988) Argon-loss by alkali feldspars. Geochimica et Cosmochimica Acta, 52, 1097–1112.

Ramseyer, K., AlDahan, A.A., Collini, B., and Landström, O. (1992) Petrological modifications in granitic rocks from the Siljan impact structure: evidence from cathodoluminescence. Tectonophysics, 216, 195–204.

Saigal, G., Morad, S., Bjørlykke, K., Egeberg, P.K., and Aagaard, P. (1988) Diagenetic albitization of detrital K-feldspar in Jurassic, Lower Cretaceous, and Tertiary clastic reservoir rocks from offshore Norway, I. Textures and origin. Journal of Sedimentary Petrology, 58, 1003–1013.

Smith, P. and Parsons, I. (1974) The alkali feldspar solvus at 1 kilobar water vapour pressure. Mineralogical Magazine, 39, 747–767.

Voll, G. (1960) New work on petrofabrics. Journal of the Liverpool and Manchester Geological Society, 2, 521–525.

Waldron, K. and Parsons, I. (1992) Feldspar microtextures and multistage thermal history of syenites from the Coldwell Complex, Ontario. Contributions to Mineralogy and Petrology, 111, 222–234.

Waldron, K., Lee, M.R., and Parsons, I. (1994) The microstructures of perthitic alkali feldspars revealed by hydrofluoric acid etching. Contributions to Mineralogy and Petrology, 116, 360–364.

Waldron, K.A., Parsons, I., and Brown, W.L. (1993) Solution-redeposition and the orthoclase-microcline transformation: evidence from granulites and relevance to ^{18}O exchange. Mineralogical Magazine, 57, 687–695.

Walker, T.E. (1984) Diagenetic albitization of potassium feldspar in arkosic sandstones: 1984 SEPM Presidential Address. Journal of Sedimentary Petrology, 54, 3–16.

Walker, F.D.L. (1990) Ion microprobe study of intragrain micropermeability in alkali feldspars. Contributions to Mineralogy and Petrology, 106, 124–128.

——— (1991) Micropores in alkali feldspars. Unpublished Ph.D. thesis, University of Edinburgh.

Walker, F.D.L., Lee, M.R., and Parsons, I. (1995) Micropores and micropermeable texture in feldspars: geological and geophysical implications. Mineralogical Magazine, 59, 507–536.

Worden, R.H., Walker, F.D.L., Parsons, I., and Brown, W.L. (1990) Development of microporosity, diffusion channels and deuteric coarsening in perthitic alkali feldspars. Contributions to Mineralogy and Petrology, 104, 507–515.

MANUSCRIPT RECEIVED JUNE 5, 1996
MANUSCRIPT ACCEPTED FEBRUARY 10, 1997